

A First Principles Predictive Model of the Pedestal Height and Width: Development, Testing, and ITER Optimization with the EPED Model

P.B. Snyder¹, R.J. Groebner¹, J.W. Hughes², T.H. Osborne¹, M. Beurskens³, A.W. Leonard¹, and H.R. Wilson⁴

¹General Atomics, P.O. Box 85608, San Diego, CA 92186-5608, USA

²MIT Plasma Science and Fusion Center, Cambridge, MA, USA

³EURATOM/UKAEA Fusion Association, Culham Science Centre, Abingdon, UK

⁴University of York, Heslington, York, UK

e-mail contact of main author: snyder@fusion.gat.com

Abstract. We develop and test a model for the H-mode pedestal height and width based upon two fundamental and calculable constraints: 1) onset of non-local peeling-ballooning modes at low to intermediate mode number, 2) onset of nearly local kinetic ballooning modes at high mode number. Calculation of these two constraints allows a unique, predictive determination of both pedestal height and width. The present version of the model is first principles, in that no parameters are taken from observation, and includes important non-ideal effects. Extensive successful comparisons to existing experiments on multiple tokamaks, including experiments where predictions were made prior to the experiment, are presented, and predictions for ITER are discussed.

1. Introduction

The pressure at the top of the edge transport barrier (or “pedestal height”) in tokamaks strongly impacts global confinement and fusion performance. Accurately predicting the pedestal height in ITER and demonstration power plants is an essential element of prediction, and a powerful tool for optimization, of fusion performance.

The spontaneous formation of the edge barrier (or “L-Mode to H-Mode transition”) creates a near-step (or “pedestal”) in the pressure profile across the radially outermost few percent of the confined plasma [Fig. 1(a)]. Pedestal formation both increases the global pressure and broadens the pressure profile, in part because of the physics of gradient-scale-length driven core turbulence, resulting in a dramatic improvement of both global confinement and global stability, with both generally increasing with the height of the pedestal.

Inside the edge barrier itself, the dynamics are complex and quite different than in the core plasma. Turbulence levels are typically much reduced from L-mode edge values. ExB shearing rates are high, and generally increase as the pedestal height increases, due to the increase in the ion diamagnetic term, which is proportional to the ion pressure gradient. In what we refer to here as “high performance” H-modes, the pedestal generally continues to rise until strong limiting instabilities are triggered, which constrain the growth of the pedestal and can determine its structure (though other mechanisms, including remnant turbulence and neoclassical transport, can be important in understanding the detailed dynamics). In this paper, we develop and test a predictive model (EPED) for the pedestal structure based on two key limiting instabilities, non-local peeling-ballooning (P-B) modes, and nearly-local kinetic ballooning modes (KBM). Combining these two constraints allows prediction of two unknowns, the pedestal height and width. These predictions can be made prior to experiments on existing devices, and can also be used to predict and optimize performance of future devices such as ITER. The present version of the model (EPED1.6) makes no use of fitting parameters or measurements, and its predictions are determined entirely from P-B and KBM theory using the computational methods described below.

The physics of the peeling-ballooning (P-B) mode is briefly described in Sec. 2, along with the method for calculating the P-B constraint in the EPED model. In Sec. 3, the KBM is described, along with the “ballooning critical pedestal” (BCP) technique used to calculate this

constraint in the EPED model. Section 4 describes the complete EPED model, both in its original (EPED1) and present (EPED1.6) versions, and Sec. 5 presents series of tests on existing devices, and predictions for ITER.

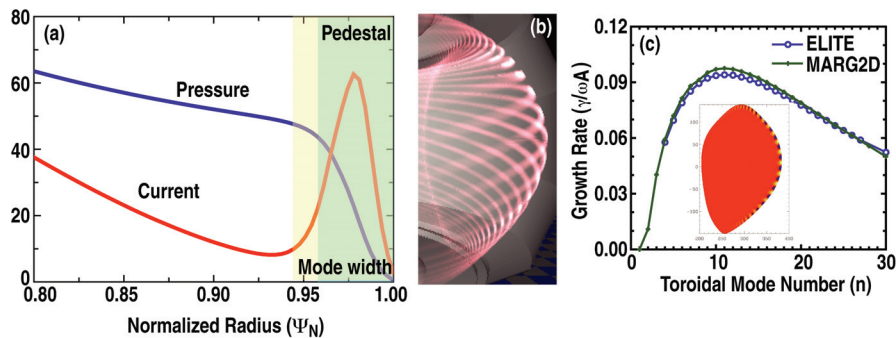


FIG. 1. (a) Illustration of typical H-mode pressure and current profiles with the edge barrier or “pedestal” region dark shaded, and the peeling-ballooning mode width (light shaded), extending across and beyond the pedestal. (b) Calculated 3D structure of an $n=18$ peeling-ballooning mode in the DIII-D tokamak. (c) Benchmark of peeling-ballooning growth rates between the ELITE and MARG2D codes for a realistic equilibrium truncated at the 99.8% flux surface. The $n=11$ 2D mode structure is inset (blue and yellow contours on orange background).

2. The Peeling-Ballooning Mode Constraint

The strong pressure gradient, and resulting large bootstrap current, in the edge barrier region [Fig. 1(a)] provide free energy to drive intermediate wavelength MHD instabilities, which are known as “peeling-ballooning” (P-B) modes, due to the coupling of the pressure-gradient driven ballooning and current-driven peeling/kink drives. While early studies of peeling-ballooning coupling employed the local, high toroidal mode number (high- n) limit [1], it is important to emphasize that these modes are fundamentally non-local in character, with significant finite- n effects, and a radial extent that is typically comparable to, or wider than, the edge barrier [2–7], as shown in Fig. 1(a). A typical 3D structure of an $n=18$ peeling-ballooning mode is shown in Fig. 1(b).

The peeling-ballooning stability boundary is evaluated by calculating mode growth rates across a broad range of toroidal mode numbers (typically $n \sim 3$ –30), with an efficient MHD code, such as ELITE [2,3,9], which has been developed and optimized specifically for this purpose. ELITE has been extensively and successfully tested against other MHD stability codes [3,5,9]. An example, showing a successful benchmark of the ELITE and MARG2D [10,11] codes, is given in Fig. 1(c).

Investigation of peeling-ballooning stability has led to improved understanding of important constraints on the pedestal height and the mechanism for edge localized modes (ELMs). The combination of high-resolution pedestal diagnostics, including substantial recent improvements, and highly efficient stability codes, has made edge stability analysis more routine on several major tokamaks, contributing both to understanding and to experimental planning and performance optimization. Extensive testing has led to substantial confidence in the accuracy of the calculated peeling-ballooning constraint on the pedestal height [e.g. 2,4-8]. A recent compilation of results on several devices [5] notes that observed maximum pedestal height and ELM onset condition agree with the calculated peeling-ballooning constraint within measurement uncertainty across a substantial sample size.

The tests of the peeling-ballooning model described above generally rely on equilibria reconstructed after experiments, incorporating profiles measured with high-resolution diagnostics, and perturbing around measured profiles to construct stability diagrams. To invoke peeling-ballooning stability predictively, we have developed a technique using model

equilibria characterized by a small set of scalar parameters [4,5]. These model equilibria are designed to have simple functional forms for the profiles, while capturing the characteristics important for peeling-ballooning stability (particularly plasma shape, pedestal profiles and bootstrap current) sufficiently to allow quantitatively accurate calculations of stability bounds. Peeling-ballooning stability studies using model equilibria successfully account for observed trends in pedestal height with plasma shape, collisionality, magnetic field (B_T), and current (I_p) [4,5]. An example is shown in Fig. 2(b), where model equilibria are used to calculate the peeling-ballooning stability limit as a function of I_p , which is then compared to data from a current scan on DIII-D.

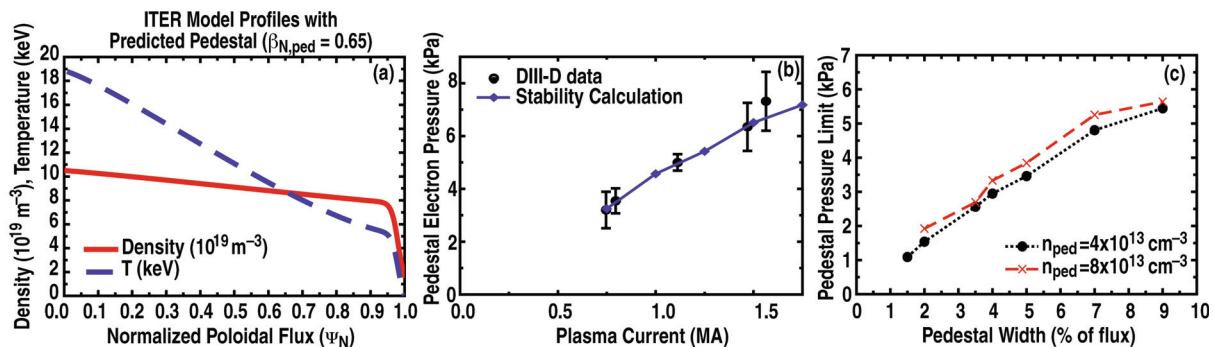


FIG. 2. (a) Temperature and density profile shapes used in the model equilibria, with tanh-shaped edge barriers. Profiles shown are for an ITER model equilibrium with $\beta_{N,ped}=0.65$. (b) Peeling-ballooning stability boundary (solid line) calculated using ELITE and model equilibria, agrees well with observed pedestal height in a DIII-D current scan. (c) Calculated peeling-ballooning stability boundary as a function of pedestal width for 2 densities shows sub-linear ($\sim \Delta_{\psi}^{3/4}$) width dependence.

In the above calculations, the width of the pedestal [$\Delta_{\psi}=0.045$ in Fig. 2(b), where Δ_{ψ} is the pedestal width in normalized poloidal flux] is an input. The peeling-ballooning stability calculation itself provides a constraint on the pedestal height as a function of the width. This relation is rather complex in general due to the non-locality of the peeling-ballooning modes; that is, it is not a simple gradient limit. However, the relationship can be readily calculated, as shown in Fig. 2(c), and generally, the peeling-ballooning constraint on the pedestal height is found to scale roughly with the $3/4$ power of the pedestal width ($\beta_{N,ped} \sim \Delta_{\psi}^{3/4}$). Hence, as the pedestal width increases, the maximum stable pedestal height increases less than linearly, and the maximum stable gradient decreases.

Using the ELITE code to evaluate $n=(5,6,8,10,15,20,30)$ stability, and a growth rate threshold determined by a model of diamagnetic stabilization, the peeling-ballooning constraint on the pedestal height can be determined as a function of the width. However, a second constraint is required in order to predict both the pedestal height and width. That second constraint is provided by KBM onset, as described in the following section.

3. The Kinetic Ballooning Mode Constraint

The EPED series of models employ local onset of the kinetic ballooning mode (KBM), as a second constraint. A simplified form of the KBM constraint is developed using a “ballooning critical pedestal” (BCP) technique, in which an edge barrier profile is taken to be ballooning critical when the central half of it is at or beyond the local ballooning threshold.

The KBM has been extensively studied in linear and nonlinear gyrofluid and gyrokinetic simulations, as well as semi-analytic treatments [e.g. 12–16]. The KBM can be considered as the kinetic analog of the local MHD ballooning mode, and has a similar threshold for instability in the limit of zero ion temperature gradient, and a somewhat lower threshold, due to ion drift resonance, at finite ion temperature gradient [12–14]. A schematic diagram of

KBM stability is shown in Fig 3a. As the plasma pressure gradient is increased (at fixed density and temperature scale length), the ion temperature gradient mode is weakly stabilized by finite- β effects, and eventually, near the MHD ballooning limit, the KBM is destabilized. The KBM onset is highly stiff, in that the growth rate becomes large at pressure gradients only marginally above the threshold. Both quasi-linear estimates and nonlinear simulations find that KBM-driven transport rises to large levels near threshold [12–16]. An example contrasting electrostatic ITG turbulence with electromagnetic KBM turbulence is shown in Fig. 3(b,c). While ITG and KBM turbulence have similar spatial scales, KBM turbulence is characterized by short correlation times and very large heat and particle transport (heat and particle diffusion coefficients normalized to gyroBohm $\gg 1$) [14].

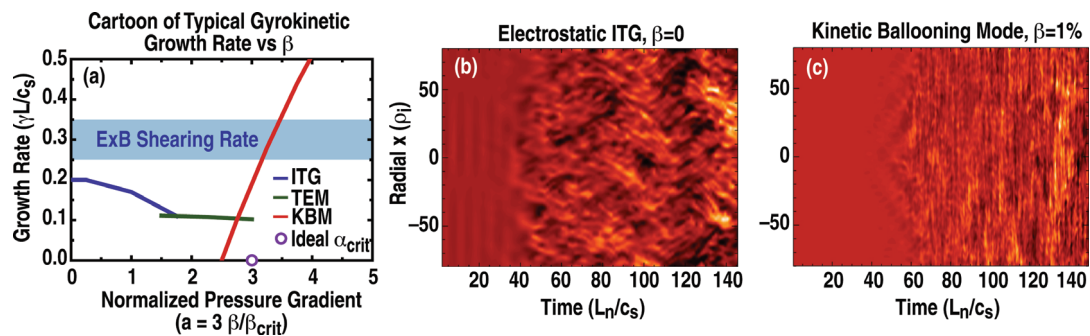


FIG. 3. (a) Schematic diagram of gyrokinetic growth rates for the ITG, TEM, and KBM as a function of normalized pressure gradient. The KBM attains a large growth rate, exceeding typical ExB shearing rates, in the vicinity of the local ballooning critical gradient (open circle). (b) Time evolution of ITG and (c) KBM turbulence from electromagnetic gyrofluid simulation [14]. The KBM exhibits short correlation times and high transport levels.

To develop a simple, numerically efficient model of the KBM constraint, we make the approximations that KBM onset is highly stiff (transport will balance sources at a gradient near the onset value), and that the onset condition can be approximated as the MHD local ballooning limit. The first approximation is well justified by simulation results, and the second is found to be surprisingly accurate (within $\sim 10\%$) in standard aspect ratio tokamaks, due to the partial offset of destabilizing (ion drift resonance) and stabilizing (FLR, ExB shear stabilization) effects. As shown in Fig. 3(a), the KBM growth rate rises to large values, where ExB shear stabilization is overcome, and large transport fluxes are driven, in the vicinity of the local MHD ballooning limit (open circle).

Criticality to the KBM provides an approximately local constraint, which we wish to integrate across the edge barrier to generate a relationship between the pedestal height and width. In principle, this integration can be performed by constructing profiles which are ballooning-critical at all radial points in the edge barrier. However, in practice, with realistic equilibria with self-consistent bootstrap current and fixed total current, this becomes a highly complex, non-local problem. A more efficient approach is to choose a simple functional form for the profiles in the edge barrier, and then increase the pedestal height at each fixed width until the profile is at or beyond criticality across half of the edge barrier (and thus, on average, approximately critical across the whole barrier). The ‘‘ballooning critical pedestal’’ (BCP) approach employs the same sets of model equilibria previously used for peeling-ballooning stability studies [Figs. 2(a), 4(a) and Refs 4, 5], which have tanh shaped density and temperature profiles in the edge barrier, and self-consistent bootstrap current calculated with the Sauter model. At each value of the pedestal width, the pedestal height is increased until the profile is at or beyond criticality across the central half of the profiles, as shown in Fig 4(a). This defines a relationship between the pedestal height and width at criticality that can be calculated as a function of the model equilibrium input parameters.

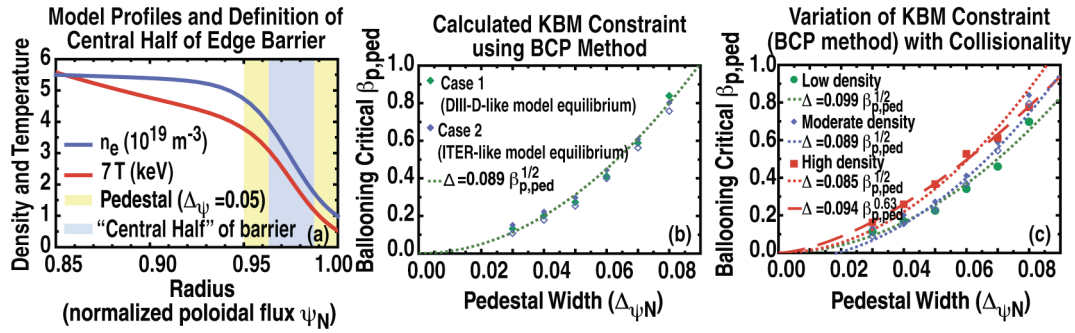


FIG. 4. (a) Edge profiles for a model equilibrium illustrate the pedestal region (light shaded) and the central half (dark shaded) of the barrier which must be at or beyond criticality in the BCP technique. (b) The KBM constraint, calculated with the BCP technique, for two different model equilibria (DIII-D-like and ITER-like) shows a dominant $\beta_{p,ped} \sim \Delta^2$, or equivalently, $\Delta \sim \beta_{p,ped}^{1/2}$, dependence (dotted line). (c) The calculated KBM constraint shows a relatively weak but complex dependence on density (i.e. collisionality).

Calculations of the KBM constraint using the BCP technique are shown in Figs 4(b,c). For each value of the pedestal width ($\Delta\psi = 0.03, 0.04, \dots, 0.08$), the pedestal height is increased until the BCP criterion is met. The filled symbols show calculations, and dashed and dotted lines show parametric fits to those calculations. Figure 4(b) shows the calculation for model equilibrium parameters typical of a DIII-D and an expected ITER discharge. Despite substantial differences in these parameters (e.g. minor radius of 0.6 m vs 2 m, major radius of 1.66 m vs 6.2 m, B_T of 2 T vs 5.3 T, I_p of 1.2 MA vs 12 MA) and associated dimensionless parameters, the KBM constraint in terms of poloidal beta at the pedestal top ($\beta_{p,ped}$) is very similar in the two cases, approximately $\Delta\psi_N = 0.089 \beta_{p,ped}^{1/2}$, as shown by the dotted line in Fig. 4(b). Note that this approximate $\Delta\psi_N \propto \beta_{p,ped}^{1/2}$ dependence is expected, due to the characteristics of ballooning stability in the bootstrap-current dominated regime of the edge barrier in standard aspect ratio shaped tokamaks [17]. Generally, the BCP calculated KBM constraint can be written in the form $\Delta\psi_N = \beta_{p,ped}^{1/2} G(\nu_*, \epsilon, \dots)$ where G is a weakly varying function of collisionality (ν_*), aspect ratio (ϵ) and other dimensionless parameters, with values typically in the range 0.07–0.1 for standard aspect ratio shaped tokamaks.

4. The EPED Pedestal Model

The peeling-ballooning and KBM constraints described in the previous two sections can then be combined to yield a predictive model (EPED) for the pedestal height and width. The inputs (\mathbf{I}) to the model are 8 scalar parameters which are used to define the model equilibria, $\mathbf{I} = [B_T(\text{T}), I_p(\text{MA}), R(\text{m}), a(\text{m}), \delta, \kappa, n_{e,ped}(10^{19} \text{ m}^{-3}), \beta_{N,global}]$, where R is the geometric major radius, a is the minor radius, δ is triangularity, κ is elongation, $n_{e,ped}$ is the pedestal electron density, and $\beta_{N,global}$ is the global Troyon normalized β . The first six input parameters, describing plasma shape and fields, are generally well known for future devices as well as future experiments on existing devices. The accuracy to which the final two parameters, which determine pedestal collisionality and global Shafranov shift, are known varies depending on the device and control methods employed. When necessary, EPED predictions can be made over a range in these parameters. The outputs of the EPED model are the pedestal height, usually given as a pressure (p_{ped}) or a normalized pedestal beta ($\beta_{N,ped}$), and the pedestal width in normalized poloidal flux ($\Delta\psi$).

An illustration of the EPED model is given in Fig. 5(a). The solid line shows the calculated P-B constraint, the dotted line is the KBM constraint, and the solid circle shows their intersection, the EPED predicted pedestal height and width. Note that the differing functional dependencies of the P-B ($p_{ped} \sim \Delta\psi^{3/4}$) and KBM ($p_{ped} \sim \Delta\psi^2$) constraints ensure a

unique nontrivial solution, and that the predicted height and width both depend on both the P-B and KBM constraints. That is, if either constraint is systematically incorrect, both the predicted height and width will be systematically incorrect, and hence both aspects of the model can be tested against measurements of the pedestal height (which is relatively easy to measure) as well as the width. Note also that the pedestal height can be maximized either by *improving* P-B stability [raising solid line in Fig. 5(a)], or, counter-intuitively, by *degrading* KBM stability (lowering dotted line). For the case shown in Fig. 5(a), EPED predictions were made before a DIII-D experiment, and the measured pedestal height and width for DIII-D shot 132010 are shown by the open symbol.

4.1 The EPED1 Model

A simple version of the EPED model, EPED1, emphasizes the dominant dependence of the KBM constraint on $\beta_{p,ped}$. As noted above, for standard aspect ratio shaped tokamaks, the BCP calculated KBM constraint takes the form $\Delta_{\psi_N} = \beta_{p,ped}^{1/2} G(v_*, \epsilon, \dots)$ where G is a weakly varying function. This constraint can be approximated by taking an ensemble average over relevant sets of input parameters \mathbf{I} . Using the BCP technique, and 16 sets of input parameters (4 each typical of DIII-D, JET, AUG and ITER), we find an ensemble average $\langle G \rangle = 0.084 \pm 0.010$. For historical reasons [17], the value $\langle G \rangle = 0.076$ is used in EPED1, leading to the simplified KBM constraint $\Delta_{\psi_{NEPED1}} = 0.076 \beta_{p,ped}^{1/2}$.

The P-B constraint in EPED1 is directly calculated using ELITE on model equilibria specified by the input parameters \mathbf{I} as described in Sec. 2. A simple model of diamagnetic stabilization is employed via a growth rate threshold $\gamma_{P-B} > \omega_{*pi}/2$, where ω_{*pi} is the half maximum value of the ion diamagnetic frequency in the edge barrier. The simplicity and efficiency of the EPED1 model have allowed it to be tested against large sets of data, including multiple experiments in which predictions were made before the experiment was conducted.

4.2 The EPED1.6 Model

In the current version of the model, EPED1.6, both the P-B and KBM constraints are directly calculated for each set of inputs \mathbf{I} , leading to a model that is first principles in the sense that all aspects are derived and no reference is made to observations.

Beyond the dominant $\Delta_{\psi_N} \propto \beta_{p,ped}^{1/2}$ dependence of the KBM constraint, additional dependencies, such as that on collisionality (v_*), can be explored using the BCP technique. An example is shown in Fig. 4(c), in which the reference pedestal density (blue diamonds) is increased by 50% (red squares) or decreased by 25% (green circles). As shown by the fits to

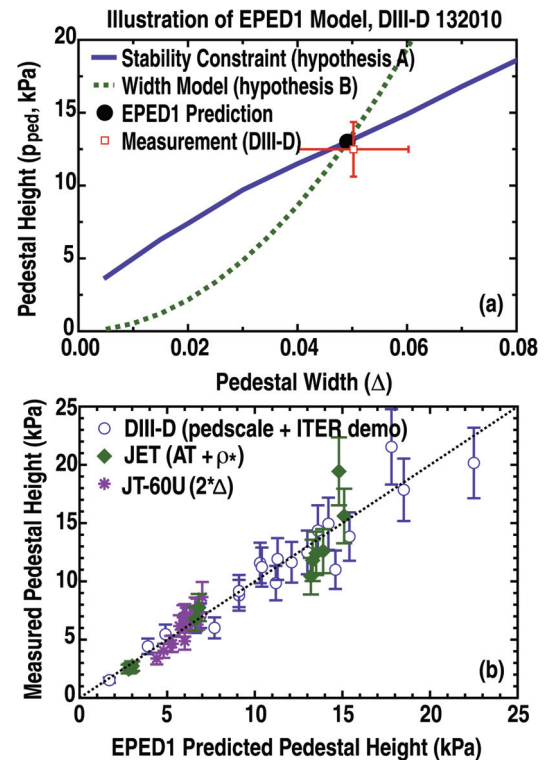


FIG. 5. (a) The EPED model predicts a pedestal height and width (solid circle) from the intersection of peeling-ballooning (solid line) and KBM (dotted line) constraints. This can then be compared with observations, here shown by an open square, for DIII-D discharge 132010 (b) The EPED1 predicted pedestal height is compared to observations on DIII-D, JET [21] and JT-60U [20], finding good agreement.

each case, both the coefficient, and at high v_* , the exponent of the KBM constraint vary somewhat with v_* . The variation with v_* is complex, depending on shape and other parameters, so a parameterization is not straightforward. Hence, in EPED1.6, the KBM constraint is calculated directly for each case with the BCP technique, allowing the secondary dependencies to be accurately accounted for (at the cost of additional complexity and computation). For each set of inputs, the BCP technique is employed at $\Delta_\psi = 0.03, 0.04, 0.05, 0.07$, and a curve fit specific to each I is used to generate the KBM constraint.

The P-B constraint is calculated with ELITE as above, with the addition of a more sophisticated diamagnetic stabilization model which accounts for the rollover in diamagnetic stabilization at high- n . This model is developed via a fit to self-consistent calculations of diamagnetic stabilization of P-B modes using the BOUT++ code [18]. An accurate model of diamagnetic stabilization is particularly important for Alcator C-Mod.

5. Experimental Tests and Predictions for ITER

The EPED model has been extensively tested across a range of experiments on several devices. A dedicated experiment to test the model was conducted on DIII-D, in which EPED1 predictions were made before the experiment, and plasma current, toroidal field and triangularity were varied by a factor of 3, to yield more than an order of magnitude variation in the pedestal height, and a factor of three variation in the pedestal width. The EPED1 model was found to be in good agreement with the observations, with a ratio of predicted to observed pedestal height of 1.03 ± 0.13 , and of width of 0.93 ± 0.15 in 17 discharges [19,17]. A comparison across a set of 21 DIII-D (the 17 mentioned above and 4 ITER demonstration discharges), 16 JT-60U [20] and 11 JET [21] discharges found a similar level of agreement (1.02 ± 0.14) as shown in Fig. 5(b). The model was also found to recover the observed variation of the pedestal height with time on JT-60U, a phenomenon attributed to relatively small variations in density and global Shafranov shift by EPED1. The EPED1 model has recently been automated, allowing comparisons to large datasets, whose results will be reported in the near future.

The new EPED1.6 model is found to accurately predict the observed pedestal height in a set of 7 DIII-D and 7 JET [21] discharges, with a large range of variation in pedestal height (1.6–22kPa), normalized gyroradius ρ_{*ped} (0.24–0.7), v_* (0.3–5), and β_{ped} (0.3%–1.2%), with a ratio of predicted to observed pedestal height of 1.02 ± 0.21 , as shown in Fig. 6(a). The model is also consistent with the observation of the lack of a positive correlation between pedestal width and gyroradius [19–22]. The inclusion of collisionality dependence in the KBM constraint, along with the improved diamagnetic stabilization model allows the EPED1.6 model to accurately predict pedestal height in ELMing discharges on Alcator C-Mod. A comparison with six C-Mod discharges from a dedicated current scan experiment finds a ratio of predicted to observed pedestal height of 1.03 ± 0.19 , shown in Fig. 6(b).

Combining the DIII-D, JET and C-Mod comparisons [Fig. 6(b)], the EPED1.6 model has been successfully tested over a factor of 23 in pedestal height. Using the model to predict the ITER pedestal height, we find an expected pedestal height of $\beta_{N,ped} \sim 0.6$, or $p_{ped} \sim 92$ kPa, less than a factor of 3 above the range studied, as shown by the black diamond in Fig. 6(b). The predicted ITER pedestal width is $\Delta_\psi \sim 0.04$ (both predictions are similar to those for EPED1, discussed in Refs [5,17]). We note that the predicted pedestal in ITER is in the low collisionality kink/peeling limited regime, where quiescent H-mode operation is possible, and pedestal height increases with density. The predicted height and width depend on the precise values chosen for the inputs I , and optimization is possible, both of the pedestal itself, and of the combined pedestal-core system, by combining EPED with global MHD calculations and a core transport model such as TGLF [23].

6. Discussion and Future Work

We have developed and successfully tested a model for the pedestal height and width in high performance H-modes based upon two fundamental and calculable constraints: 1) onset of non-local P-B modes at low to intermediate mode number, 2) onset of nearly-local kinetic ballooning modes at high mode number. The present version of the model, EPED1.6, calculates both constraints directly, has no parameters fit to observation, and accurately predicts the pedestal height in a set of 20 DIII-D, JET and C-Mod discharges (ratio of 1.02 ± 0.20 and correlation coefficient of 0.96 between predicted and observed pedestal height).

Predictions are made for the pedestal height and width in ITER, and a full optimization study, including coupling to core MHD and transport, is underway. Initial indications are that, with proper optimization, ITER should be able to achieve its $Q=10$ objective. ITER will face the additional challenge of avoiding large ELMs while operating with a high pedestal. Fortunately, the ITER pedestal is predicted to be in the low collisionality kink/peeling limited regime where both ELM-free quiescent H-mode and resonant magnetic perturbation ELM suppression have been demonstrated.

Development of the EPED model is ongoing, with a fully gyrokinetic version of the BCP technique planned to improve accuracy, especially for low aspect ratio, very strongly shaped discharges. Additional dedicated tests on multiple devices are planned.

This work was supported in part by the US Department of Energy under DE-FG03-95ER54309, DE-AC05-00OR22725, DE-FG02-92ER54141, and DE-FC02-99ER54512.

- [1] CONNOR, J.W. *et al.*, Phys. Plasmas **5** (1998) 2687
- [2] SNYDER, P. B. *et al.*, Phys. Plasmas **9** (2002) 2037
- [3] WILSON, H.R. *et al.*, Phys. Plasmas **9** (2002) 1277
- [4] SNYDER, P.B. *et al.*, Plasma Phys. Control. Fusion **46** (2004) A131
- [5] SNYDER, P.B. *et al.*, Nucl. Fusion **49** (2009) 085035
- [6] HUYSMANS, G.T.A., Plasma Phys. Control. Fusion **47** (2005) B165
- [7] WILSON, H.R. *et al.*, Plasma Phys. Control. Fusion **48** (2006) A71
- [8] SAARELMA, S. *et al.*, Plasma Phys. Control. Fusion **51** (2009) 035001
- [9] SNYDER, P.B. *et al.*, Nucl. Fusion **47** (2007) 961
- [10] AIBA, N. *et al.*, Comput. Phys. Commun. **175** (2006) 269
- [11] AIBA, N. *et al.*, Nucl. Fusion **49** (2009) 065015
- [12] REWOLDT, G. *et al.*, Phys. Fluids **30** (1987) 8017
- [13] HONG, B.-G. *et al.*, Phys. Fluids B **1** (1980) 1589
- [14] SNYDER, P.B. and HAMMETT, G.W., Phys. Plasmas **8** (2001) 744; SNYDER, P.B., PhD thesis, Princeton University (1999)
- [15] JENKO, F. and DORLAND, W., Plasma Phys. Control. Fusion **43** (2001) A131
- [16] CANDY, J., Phys. Plasmas **12** (2005) 072307
- [17] SNYDER, P.B. *et al.*, Phys. Plasmas **16** (2009) 056118
- [18] DUDSON, B.D. *et al.*, Comput. Phys. Comm. **180** (2009) 1467
- [19] GROEBNER, R.J. *et al.*, Nucl. Fusion **49** (2009) 085037
- [20] URANO, H. *et al.*, Nucl. Fusion **48** (2008) 045008
- [21] BEURSKENS, M. *et al.*, Plasma Phys. Control. Fusion **51** (2009) 124051; Nucl. Fusion **48** (2008) 095004
- [22] OSBORNE, T.H. *et al.*, this conference, EXC/2-1.
- [23] KINSEY, J.E. *et al.*, this conference, THC/3-3.

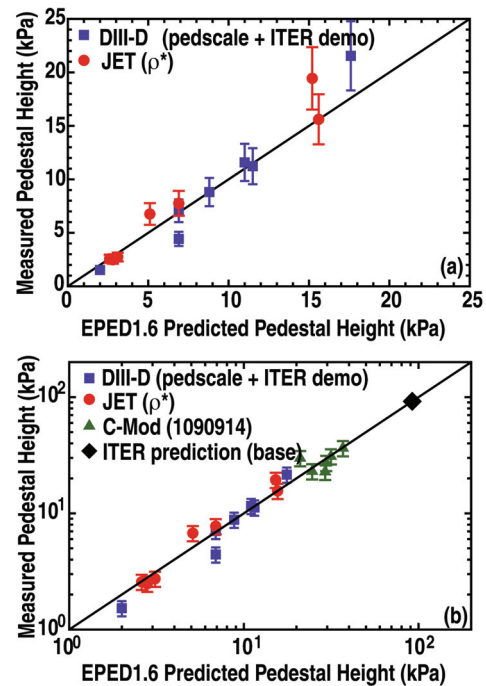


FIG. 6. (a) Comparison of EPED1.6 predicted pedestal height to measurements on 14 DIII-D and JET discharges. (b) Comparison of EPED1.6 predicted pedestal height to measurements on C-Mod, DIII-D, and JET, including prediction for ITER base case (black diamond), using a log scale.